Electronic Supplementary Material (ESI)

Hierarchically porous Fe-N-C derived from covalent-organic material as highly efficient electrocatalyst for Oxygen Reduction†

Quan Zuo,[a] Pingping Zhao,[a] Wei Luo[a,b,c]* and Gongzhen Cheng[a]*

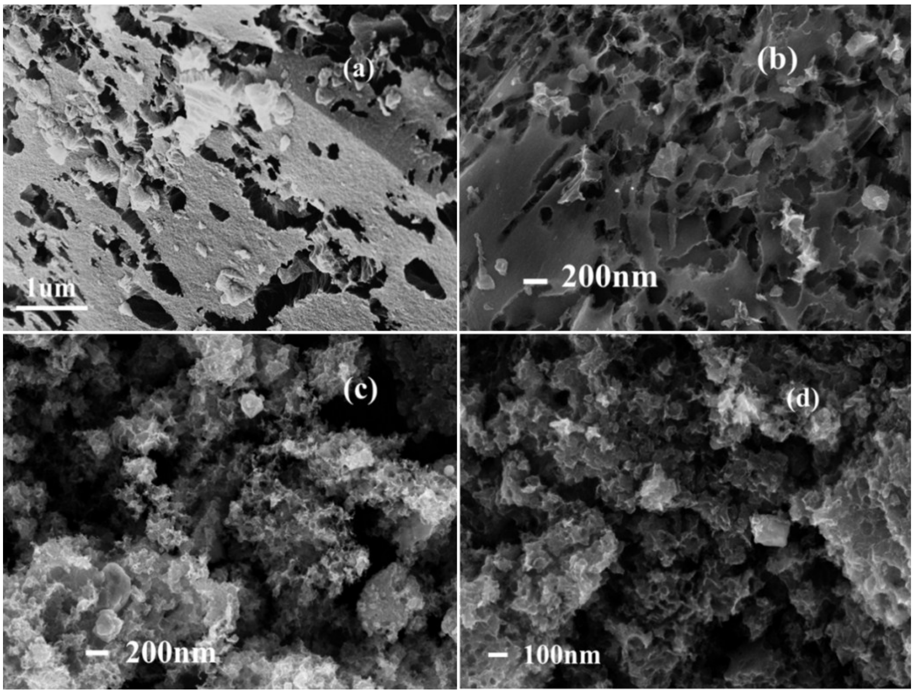

Fig. S1. SEM images of the catalysts pyrolysis at different target temperatures. (a, b) FeNC-800 (c, d) FeNC-1000

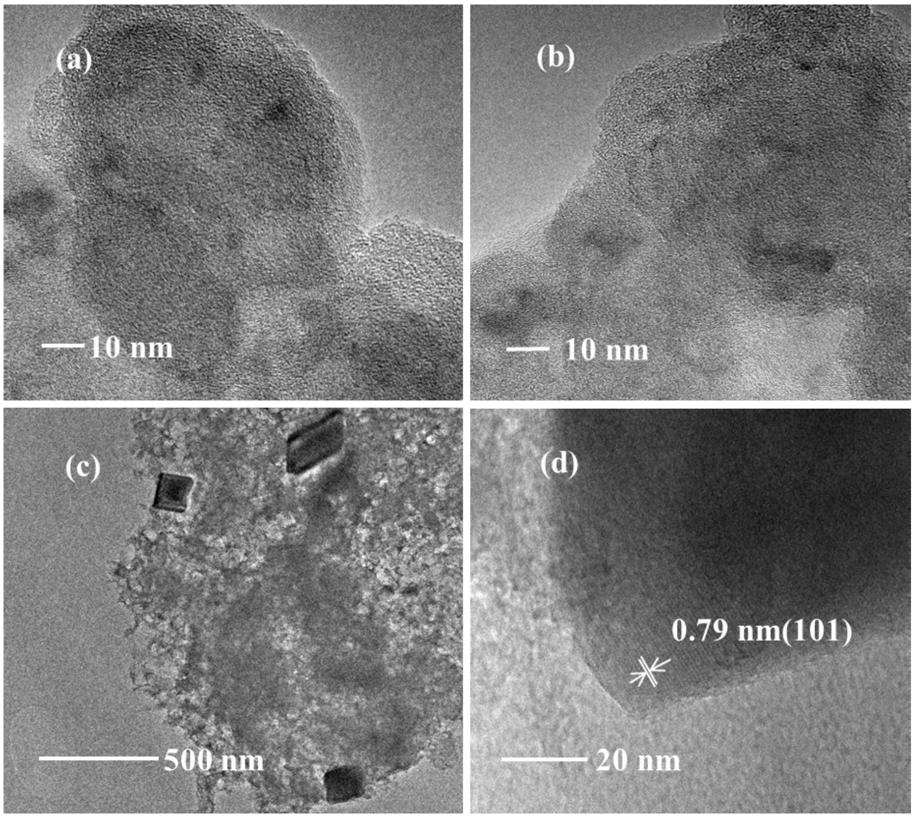

Fig. S2. TEM images of (a, b) FeNC-800 (c, d) FeNC-1000

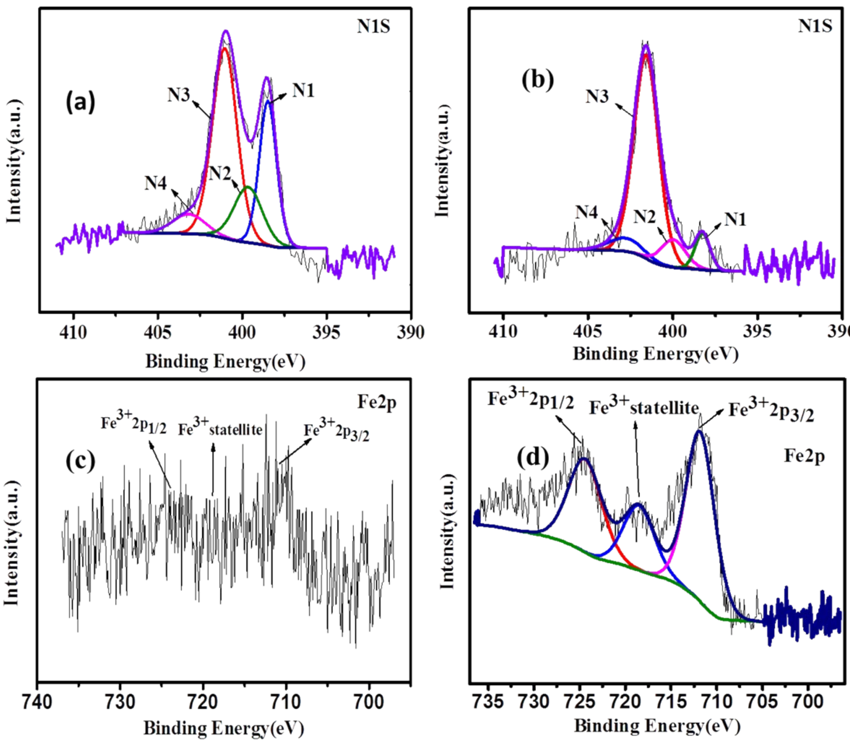

Fig. S3. The high-resolution N 1s and Fe 2p spectrum of (a, c) FeNC-800, (b, d) FeNC-1000

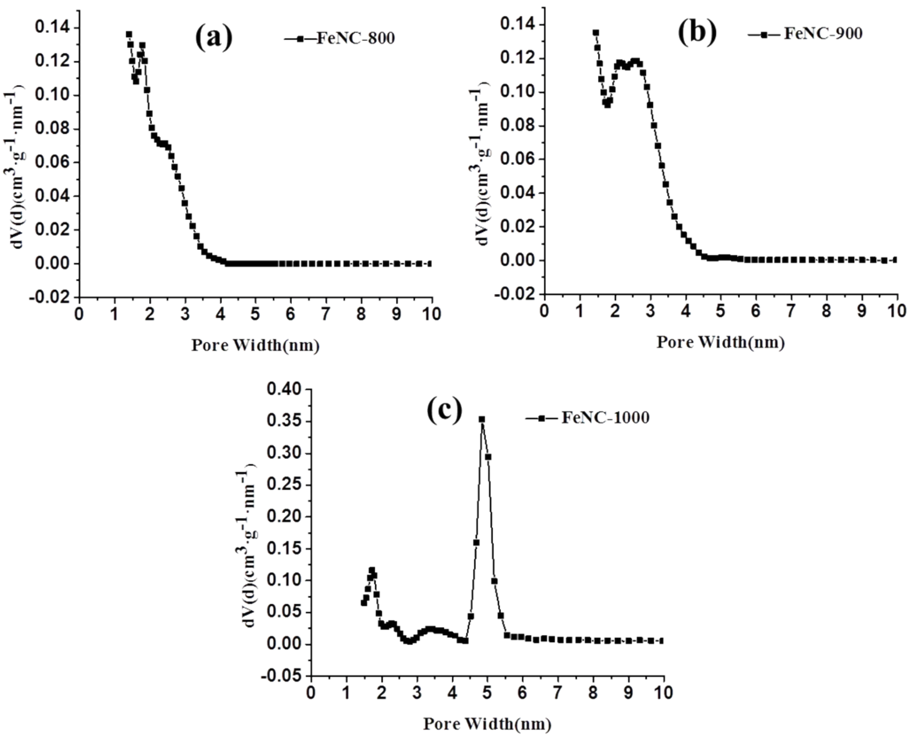

Fig. S4.   Pore size distribution of FeNC-based catalysts

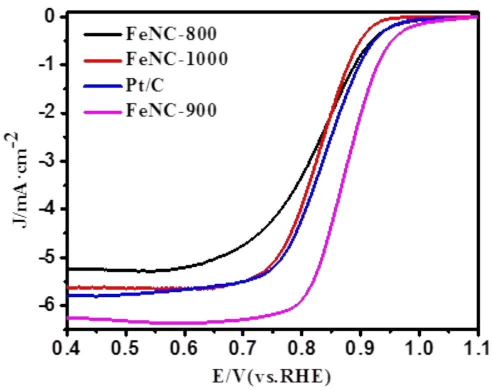

Fig. S5. Steady-state polarization curves of FeNC-based catalysts.

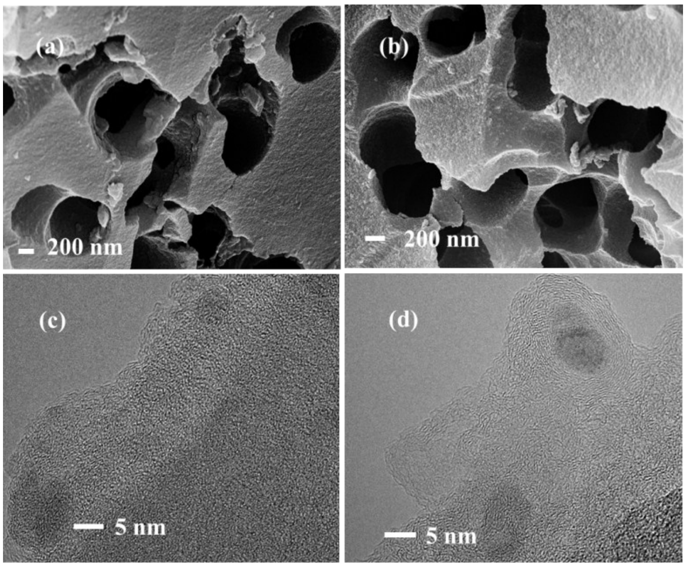

Fig. S6. SEM images of the FeNC-900 catalyst after accelerated durability test: (a) in 1M KOH solution, (b) in 1M $HClO_4$ solution.

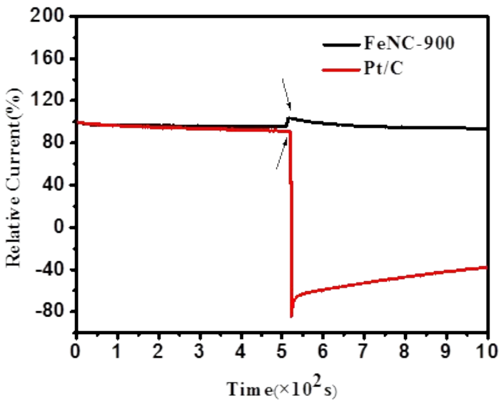

Fig. S7. Methanol-tolerance evaluation of FeNC-900 tested by the current–time chronoamperometric responses at 0.6 V versus RHE in O_2 -saturated (commercial 20% Pt/C is used for comparison) in 0.1 M KOH solution. The arrow represents the addition of 3 M methanol into the electrolyte.

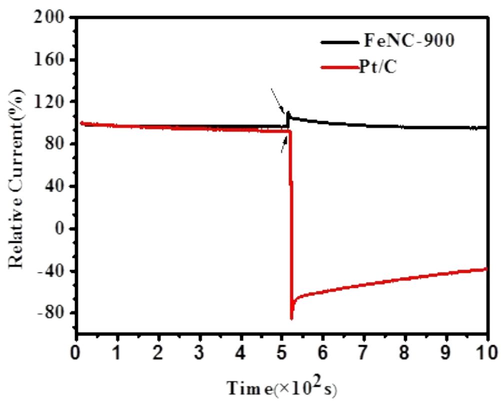

Fig. S8. Methanol-tolerance evaluation of FeNC-900 tested by the current–time chronoamperometric responses at 0.6 V versus RHE in O_2 -saturated (commercial 20% Pt/C is used for comparison) in 0.1 M $HClO_4$ solution. The arrow represents the addition of 3 M methanol into the electrolyte.

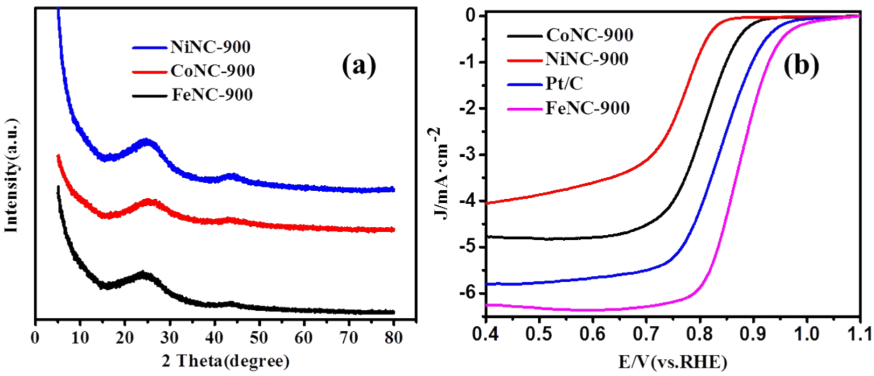

Fig. S9. (a) XRD and (b) Steady-state polarization curves of ORR of catalysts in 0.1 M KOH solution from different metal.

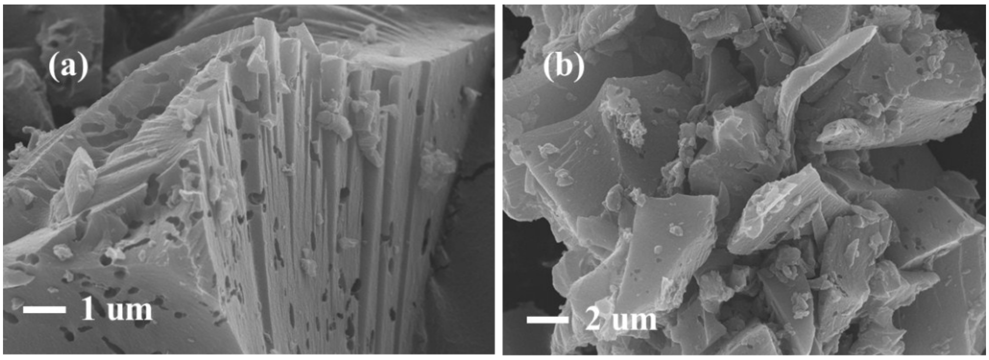

Fig. S10. SEM images of the catalysts (a) CoNC-900 and (b) NiNC-900.

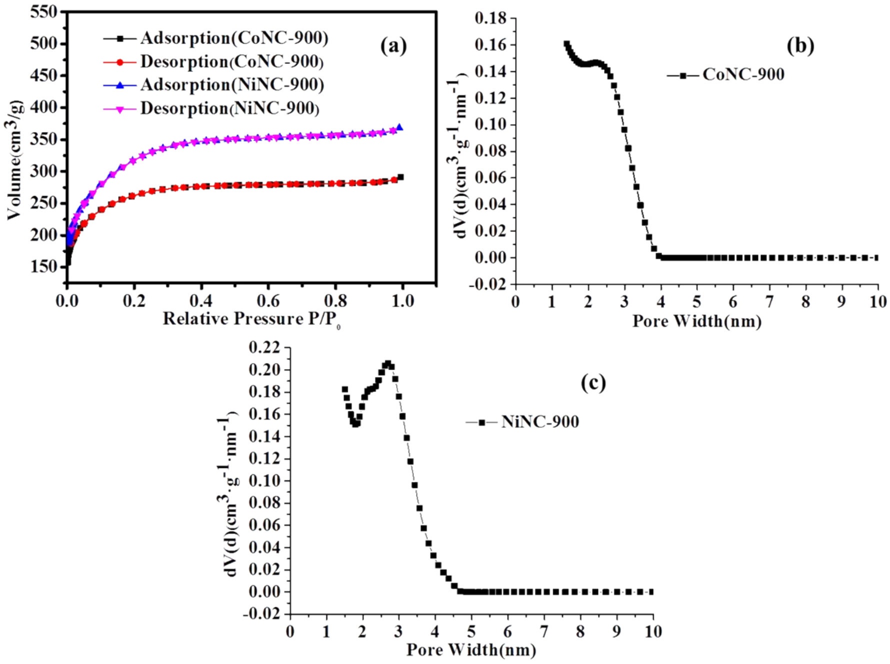

Fig. S11. (a) N_2 adsorption-desorption isotherms of CoNC-900 and NiNC-900 catalyst, (b) Pore size distribution of CoNC-900 catalyst, (C) Pore size distribution of NiNC-900 catalyst.

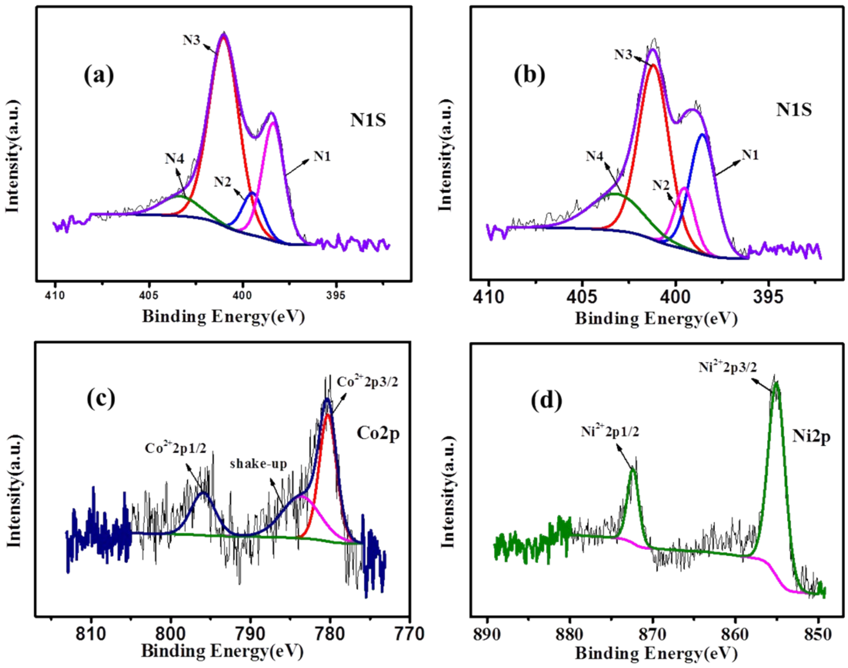

Fig. S12. The high-resolution N 1s and Co 2p (Ni 2p) spectrum of (a, c) CoNC-900, (b, d) NiNC-900

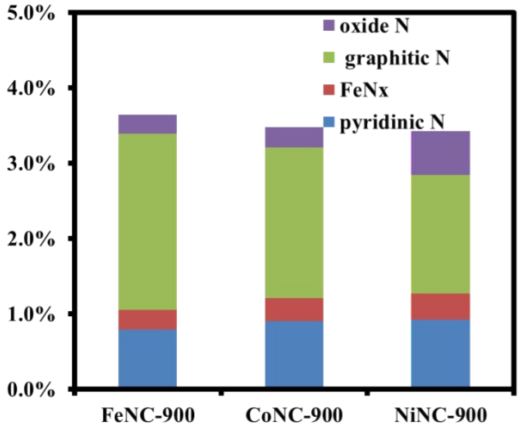

Fig. S13. The content of different N in the catalysts.

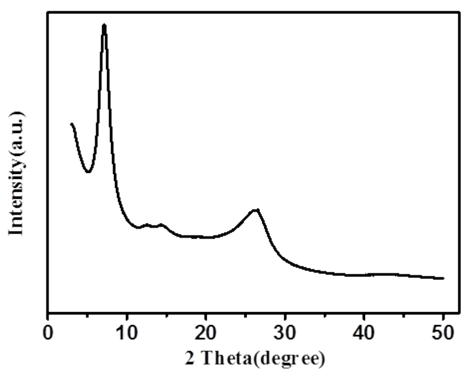

Fig. S14. XRD of CTF

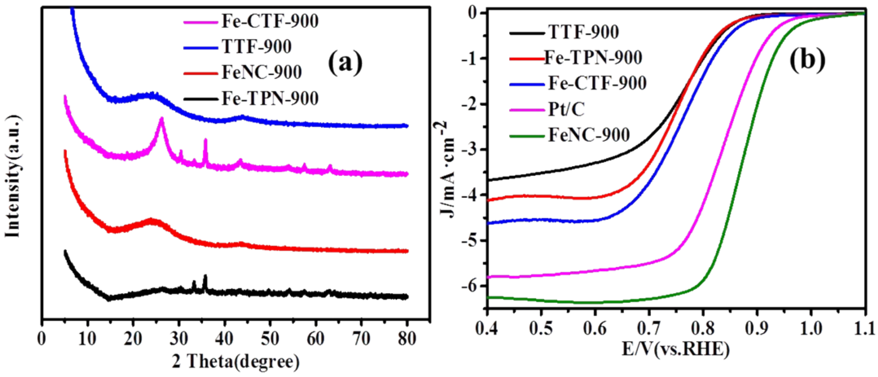

Fig. S15. (a) XRD and (b) Steady-state polarization curves of ORR of catalysts in 0.1 M KOH solution from different precursors.

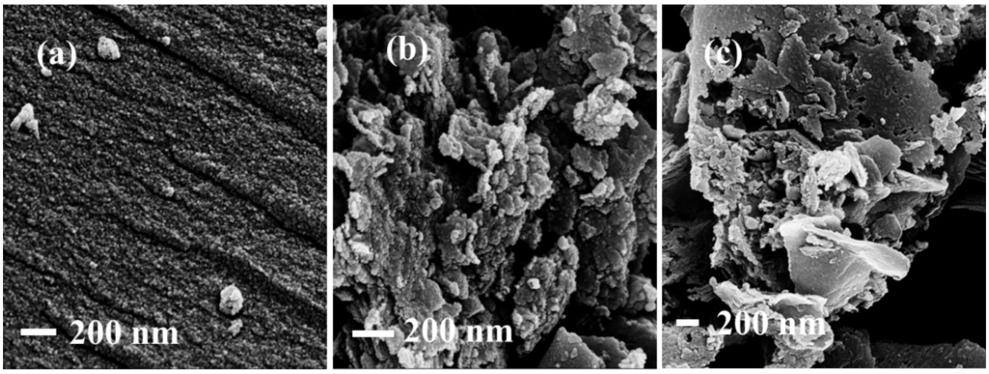

Fig. S16. SEM images of the catalysts (a) TTF-900, (b) Fe-TPN-900 and (c) Fe-CTF-900.

Table S1. Comparison of ORR catalytic performances in alkaline solution between FeNC-900 and other noble-metal-free electrocatalysts reported previously.

Catalyst	Onset potential (V vs. RHE)	Half-wave potential (V vs. RHE)	The diffusion-limited current density (mA/cm^2)	Ref.
FeNC-900	1.00	0.88	6.25	This work
Fe-N/C-800	0.98	0.81	4.81	[1]
Fe-N/C-800	0.92	0.81	6.06	[2]
Fe-N-C	0.95	0.86	6.60	[3]
Fe-N/G	0.87	0.78	5.21	[4]
Co-N-HPC	0.91	0.83	5.00	[5]
N:C-MgNTA	0.89	0.75	5.70	[6]
NCNTFs	0.95	0.87	5.30	[7]
NPC-F	0.94	0.84	5.50	[8]
Fe_2N/N-GAs-20	1.02	0.88	4.80	[9]

pPMF-800	1.05	0.88	6.20	[10]

Table S2. Comparison of ORR catalytic performances in acid solution between FeNC-900 and other noble-metal-free electrocatalysts reported previously.

Catalyst	Onset potential (V vs. RHE)	Half-wave potential (V vs. RHE)	The diffusion-limited current density (mA/cm2)	Ref.
FeNC-900	0.85	0.72	5.95	This work
Fe-N/C-800	0.80	0.68	6.09	[2]
Fe2N/N-GAs-20	0.82	0.65	3.79	[9]
pPMF-800	0.89	0.71	6.10	[10]
Fe/Co-CMP-800	0.88	0.76	4.70	[11]
Co-N-C	0.85	0.76	5.90	[12]
Co-Zn-ZIF/GO-800	0.85	0.70	4.20	[13]
H–Fe@N–C/RGO	0.89	0.67	7.80	[14]
Fe-N/C-900	0.58 (V vs. Ag/AgCl)	0.40 (V vs. Ag/AgCl)	5.78	[15]

Notes and references

1 W. Niu, L. Li, X. Liu, N. Wang, J. Liu, W. Zhou, Z. Tang and S. Chen, *J. Am. Chem. Soc*., 2015, **137**, 5555−5562.

2 L. Lin, Q. Zhu and A. Xu, *J. Am. Chem. Soc.*, 2014, **136**, 11027−11033.

3 J. Sanetuntikul and S. Shanmugam, *Nanoscale*, 2015, **7**, 7644−7650.

4 Q. Lai and Q. Su, *ACS Appl. Mater. Inter.*, 2015, **7**, 18170–18178.

5 M. Dou, D. He, W. Shao, H. Liu, F. Wang and L. Dai, *Chem. Eur. J.*, 2016, **22**, 2896–2901.

6 D. Eisenberg, W. Stroek, N. J. Geels, C. S. Sandu, A. Heller, N. Yan and G. Rothenberg, *Chem. Eur. J.*, 2016, **22**, 501−505.

7 B. Y. Xia, Y. Yan, N. Li, H. B. Wu, X. W. Lou and X. Wang, *Nature Energy*, 2016, **1**, 1−8.

8 Z. Xu, X. Zhuang, C. Yang, J. Cao, Z. Yao, Y Tang, J. Jiang, D. Wu and X. Feng, *Adv. Mater.*, 2016, **28**, 1981−1987.

9 L. Liu, X. Yang, N. Ma, H. Liu , Y. Xia, C. Chen, D. Yang and X. Yao, *Small*, 2016, **12**, 1295−1301.

10 W. Yang, X. Yue, X. Liu, L. Chen, J. Jia and S. Guo, *Nanoscale*, 2016, **8**, 959−964.

11 S. Br¨uller, H. Liang, U. I. Kramm, J. W. Krumpfer, X. Feng and K. M¨ullen, *J. Mater. Chem. A*, 2015, **3**, 23799−23808.

12 B. You, N. Jiang, M. Sheng, W. S. Drisdell, J. Yano and Y. Sun, *ACS Catal.*, 2015, **5**, 7068−7076.

13 J. Wei, Y. Hu, Y. Liang , B. Kong, J. Zhang, J. Song, Q. Bao, G. P. Simon, S. P. Jiang and H. Wang, *Adv. Funct. Mater.*, 2015, **25**, 5768–5777.

14 J. Wang, G. Wang, S. Miao, J. Liab and X. Bao, *Faraday Discuss.*, 2014, **176**, 135–151.

15 M. Yang, H. Chen, D. Yang a, Y. Gao and H. Li, *J. Power Sources*, 2016, **307**, 152−159.